Electrochimica Acta 252 (2017) 549–557

Contents lists available at ScienceDirect

Electrochimica Acta

journal homepage: www.elsevier.com/locate/electacta

Hydrothermally grown α-MnO_2 nanorods as highly efficient low cost counter-electrode material for dye-sensitized solar cells and electrochemical sensing applications

Khursheed Ahmad[a], Akbar Mohammad[a], Shaikh M. Mobin[a,b,c,*]

[a] Discipline of Chemistry, Indian Institute of Technology Indore, Simrol, Khandwa Road, Indore 453552, India
[b] Centre for Biosciences and Bio-Medical Engineering, Indian Institute of Technology Indore, Simrol, Khandwa Road, Indore 453552, India
[c] Discipline of Metallurgy Engineering and Materials Science, Indian Institute of Technology Indore, Simrol, Khandwa Road, Indore 453552, India

ARTICLE INFO

Article history:
Received 4 August 2017
Received in revised form 30 August 2017
Accepted 2 September 2017
Available online 6 September 2017

Keywords:
α-MnO_2 nanorods
counter electrode
dye sensitized solar cell
nitroaromatic sensor and electrochemistry

ABSTRACT

Multipurpose α-MnO_2 nanorods were synthesized by facile hydrothermal method. The synthesized α-MnO_2 nanorods were characterized by PXRD, UV-*vis*, SEM, EDX, TEM and SAED pattern to confirm their purity and morphology. These α-MnO_2 nanorods were employed as a low cost counter electrode in dye sensitized solar cell (DSSC) and sensor for the detection of nitroaromatic compounds. DSSC device using α-MnO_2 nanorods as counter electrode exhibited excellent power conversion efficiency (PCE) of 4.1% with 0.75 V (Voc) and 0.38 (FF). Furthermore, active surface area of the glassy carbon electrode (GCE) was modified by α-MnO_2 nanorods (**GCE/α-MnO_2**) which showed a rapid sensitivity towards *p*-nitrotoluene (*p*-NT), 2, 4-dinitrotoluene (DNT) and 2, 4, 6-trinitrophenol (TNP) with distinct cathodic peaks. The **GCE/α-MnO_2** exhibited the limit of detection (LOD) of 144 nM, 133 nM, 100 nM and a high sensitivity of 17.6 $\mu A \mu M^{-1} cm^{-2}$, 22.6 $\mu A \mu M^{-1} cm^{-2}$, 54.82 $\mu A \mu M^{-1} cm^{-2}$ for *p*-NT, DNT and TNP, respectively.

1. Introduction

In present scenario some major challenges which need immediate attention are energy crisis, environmental pollution and security threats [1]. To deal with the energy crisis, the dye sensitized solar cells (DSSCs) have been commonly employed because of their easy fabrication, high efficiency and economical viabilities as compared to conventional solar cells [2–5]. Enormous efforts have been made to further reduce the cost of the DSSCs by introducing low cost electrode materials like reduced graphene oxide (rGO), Mn_3O_4, polythiophene, nickel sulfide, carbon materials, inorganic compounds, carbide, nitride and conducting polymers etc. instead of precious metal based Pt as counter electrode [6–8]. Moreover, attempts are in progress to further improve the performances of the DSSCs by varying the fabrication methods and by tuning the morphology of counter electrode materials.

On the other hand, the presence of trace amount of nitroaromatics compounds which are responsible for high oxidation rate may lead to severe environmental, health and safety intimidations [9–13]. Thus, detection of trace amount of nitroaromatic compounds is a daunting task. Among various nitroaromatic compounds, 2,4,6-trinitrophenol(TNP) has been widely used as an explosives. Previously, there exists some reports on development of a sensor for hazardous/explosive materials by employing conventional methods like fluorescence, gas chromatography, capillary electrophoresis, ion mobility spectrometry (IMS), high performance liquid chromatography and mass spectrometry [14–19]. Owing to the presence of electrochemically active nitro functionalities which can be easily reduced to nitroso or hydroxylamine derivatives, has prompted researcher to introduce electrochemical methods. The electrochemical method possesses several advantages such as low-cost instrumentation, fast detection and the potential to develop on-site portable devices. There are a few reports available for the electrochemical detection of nitroaromatics using different nanomaterials such as N-doped rGO/CuS composite, functionalized reduced graphene oxide, rGO/Au nanocomposite and sonogel carbon) [12,13,20]. However, most of these reported sensors have the following limitations: i) use of binders, ii) enzymes, iii) expensive metals such Pd, Ag, Au or Pt, iv) sensitivity/selectivity and v) lack of distinct identification of each $-NO_2$ group present in the nitroaromatics compounds. Thus, development of multi-tasking, highly

* Corresponding author at: Discipline of Chemistry, Indian Institute of Technology Indore, Simrol, Khandwa Road, Indore 453552 India.
E-mail address: xray@iiti.ac.in (S.M. Mobin).

http://dx.doi.org/10.1016/j.electacta.2017.09.010
0013-4686/

efficient nanomaterial for dye sensitized solar cells and highly selective and sensitive electrochemical sensor for the detection of nitroaromatics still remains a challenging task.

Manganese dioxide (MnO_2) has gained much interest due to the fact of its environmental compatibility, easy availability and low cost. This enables MnO_2 as potential candidate for various applications such as Li-ion batteries [21–23], supercapacitors [24–26], sensors and catalysts [27].

Herein, we report α-MnO_2 in a dual role viz. as efficient counter electrode material for DSSCs and electrode modifier for the fabrication of a binder free non-enzymatic nitroaromatics sensor.

2. Materials and Methods

Cautions: The studied nitroaromatic compounds {*para*-nitrotoluene (*p*-NT), 2,4-dinitrotoluene (DNT) and 2,4,6-trinitrophenol (TNP)} are highly toxic/explosives. The solutions should be prepared in very low concentration and handled with great care with proper precautions (For more details on handling, see MSDS sheet).

2.1. Chemicals and reagents

All the chemicals and reagents were purchased from Solaronix, Sigma and Alfa Aesar which were used without further any purification.

2.2. Instrumental

The powder X-ray diffraction patterns (PXRD) were recorded on a Rigaku, Japan, RINT 2500 V x-ray diffractometer with Cu Kα irradiation (λ = 1.5406 Å). The morphologies and elemental constituents of the samples were characterized using Supra 55 Zeiss Field Emission Scanning Electron microscope (FESEM) attached with Energy Dispersive X-ray (EDX) spectroscopy (Oxford Instrument' X-max, AZtec). Further, more information about the morphological characteristics and size were examined by Transmission Electron Microscopy (TEM) using FEI Tecnai G2 12 Twin TEM 120 kV. The N_2 adsorption-desorption isotherm study were performed using Brunauer-Emmett-Teller (BET) method tested on Autosorb iQ with version 1.11 (Quantachrome Instruments). The performance of the fabricated DSSC device was measured by using Metrohm PGSTAT204N Autolab associated with sun light system (xenon arc lamp) under1.5 illuminations (100 mW/cm^2). All electrochemical measurements were performed on Metrohm Autolab PGSTAT 204N using NOVA software version 1.10. The GCE as a working electrode, platinum wire as a counter electrode and Ag/AgCl as a reference electrode were used for all electrochemical measurements.

2.3. Synthesis of α-MnO_2 nanorods

Potassium permanganate ($KMnO_4$; 3.0 mmol) was dissolved in deionized (D.I.) water (15 mL) under stirring for half an hour [28]. To this solution, HCl solution (12.5 mmol) was added and stirred further for 1 h (Scheme 1). The reaction mixture was then transferred into a 23 ml capacity of Teflon-lined stainless steel autoclave and kept at 180 °C for 8 h and cooled down to room temperature. The black precipitate was collected by centrifugation at 7000 rpm for 10 min and repeatedly washed with D.I. water several times and dried overnight at 60 °C.

2.4. Fabrication of the DSSC device

100 mg of α-MnO_2 nanorods was mixed in 25 mg of polyethylene glycol and ethanol which was further stirred to form a fluid mixture. α-MnO_2 nanorods film was deposited using doctor blade on FTO glass substrate and calcined for 2 h at 450 °C to obtain the counter electrode. TiO_2 layer (Solaronix, Ti-Nanoxide) was also deposited on FTO glass substrate and calcined at 450 °C for 2 h and subsequently, soaked in N-719 dye solution for 24 h to get the DSSC electrodes. The liquid electrolyte was injected between the TiO_2 electrode and counter electrode to assemble the DSSC. The liquid electrolyte was prepared by mixing 0.05 M I_2, 0.6 M 1,2-dimethyl-3-propyllimidazolium iodide, 0.1 M LiI and 0.5 M tert-butyl pyridine in acetonitrile. Surlyn 1702 and paraffin were used as the spacer between the electrodes and sealant to prevent from the leakage of the electrolyte respectively.

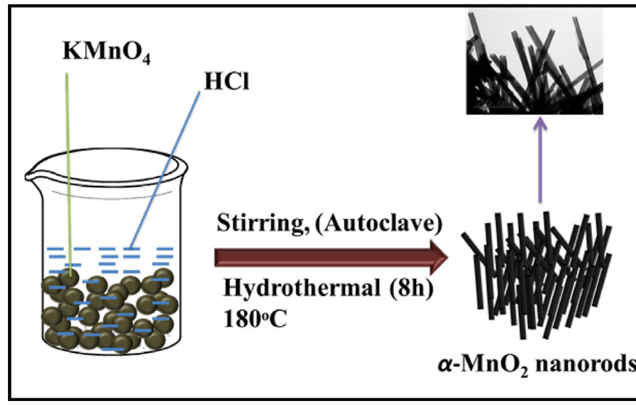

Scheme 1. Schematic diagram showing the synthesis of α-MnO_2 nanorods.

2.5. Fabrication of the explosive sensor

The glassy carbon electrode (GCE) was polished with alumina slurry and sonicated for 20 minutes to remove any residual impurity. 10 µl of α-MnO_2 nanorods solution was drop casted onto the GCE electrode and dried at room temperature for 4 h.

3. Results and Discussion

3.1. Characterization of α-MnO_2 nanorods

The phase purity and crystallinity of the synthesized α-MnO_2 nanorods were analyzed by PXRD in the 2θ range of 10–80°. The PXRD pattern of the synthesized α-MnO_2 nanorods exhibited well-defined diffraction peaks in agreement with the reported crystalline α-MnO_2 nanorods from JCPDS data (card no. 44-0141). The diffraction peaks emerged at (12.7°), (18.03°), (25.5°), (28.8°), (36.6°), (37.6°), (38.7°), (41.1°), (49.8°), (56.3°), (60.3°), (65.5°), (69.1°) and (72.6°) corresponded to the (110), (200), (220), (310), (400), (211), (301), (510), (411), (600), (521), (002), (541) and (312) planes, respectively (Fig. 1). The intense and sharp observed peaks indicated the presence of α-MnO_2 nanorods in highly, crystalline and pure form whereas no considerable diffraction peak of impurity was detected which confirmed the phase purity. The average crystallite size of α-MnO_2 nanorods was calculated to be ~33.2 nm by using Debye–Scherrer equation from PXRD patterns. The morphologies and structures of the α-MnO_2 nanorods were investigated by using SEM and TEM (Fig. 2). SEM images clearly showed the presence of α-MnO_2 composed of nanorods with smooth and uniform characteristics (Fig. 2(A-B)). The synthesized α-MnO_2 nanorods were present with average diameter of 137.1 nm and average length of 1.66 µm with clean and smooth surface (Fig. S1). Further, in order to validate that the synthesized α-MnO_2 are nanorods, they were analyzed by TEM analysis. Figs. 2(C-D) displayed the typical TEM images of the α-MnO_2 nanorods. The

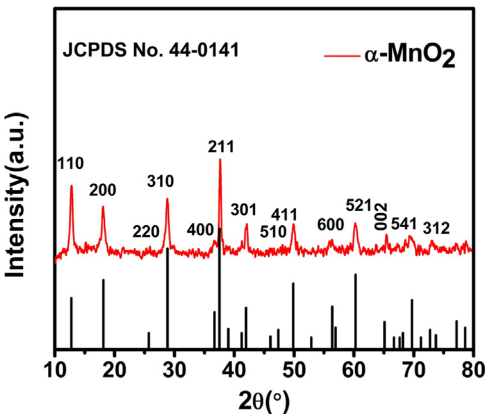

Fig. 1. PXRD of α-MnO_2 nanorods.

obtained results clearly showed the presence of α-MnO_2 with nanorods like structure which was in agreement with SEM results. The selected area electron diffraction (SAED) pattern placed in the inset of Fig. 2(D) revealed well-defined, ordered diffraction pattern with several bright spots that showed the presence of crystalline nature of obtained α-MnO_2. Further, to investigate the presence of elements in the α-MnO_2 nanorods, EDX analysis was done. EDX spectrum was recorded by EDX analysis (Fig. 3(A-B)) and presence of Mn and O were found to be 60.93 wt% and 39.07 wt% respectively (Fig. 3(B)). The specific surface area and porosity of the nanomaterials play an important role to enhance the electrocatalytic performance of the electrochemical devices [29]. The N_2 adsorption-desorption isotherm and total pore size volume of the α-MnO_2 nanorods are shown in Figs. 3(C) and 3(D), respectively. The isotherm curve of α-MnO_2 nanorods represent type III isotherm which indicate mesoporous nature of the α-MnO_2 nanorods. The α-MnO_2 nanorods showed BET surface area of 97.5 m^2/g with an average pore diameter of 3.5 nm and pore volume of 0.403 cm^3/g. The optical behavior of the α-MnO_2 nanorods was characterized by using UV-*vis* spectroscopy. Fig. 4 showed UV-*vis* spectrum of α-MnO_2 nanorods with a broad absorption peak at ~490 nm and the band gap of 2.5 eV as calculated by Tauc relation. In DSSC, the nanomaterials with different morphology influence electrocatalytic reactions which take place on the surface of the counter electrodes [30]. The high crystallinity, large surface area, high porosity, narrow band gap and the nanorod morphology of the α-MnO_2 facilitates the charge transfer from its surface (counter electrode) to the redox electrolyte (triiodide redox couple) to enhance the performance of the DSSC [30,31]. Additionally, the mesoporous structure of the α-MnO_2 nanorods provides effective electron transport networks which encourage the collection/transfer of electrons from the external circuit and later regeneration of the redox couple [32]. All these excellent properties of synthesized α-MnO_2 nanorods advocate its potential candidature as electrocatalyst for photovoltaic and sensing applications.

3.2. Photovoltaic performance of DSSC device

The electrochemical impedance spectroscopy (EIS) is widely used to investigate the electrochemical behavior of the counter electrodes. Fig. S2(A) showed the Nyquist plots for the fabricated counter electrodes with equivalent circuit presented in inset of Fig. S2(A). The obtained data from the EIS has been summarized in Table S1. The electrocatalytic performance of the counter electrode in triiodide solution could be explained by charge transfer resistance (Rct). The counter electrode with Pt showed excellent electrocatalytic activity with an Rct value of 11.47(Ω) whereas the counter electrode with α-MnO_2 nanorods showed an Rct value of

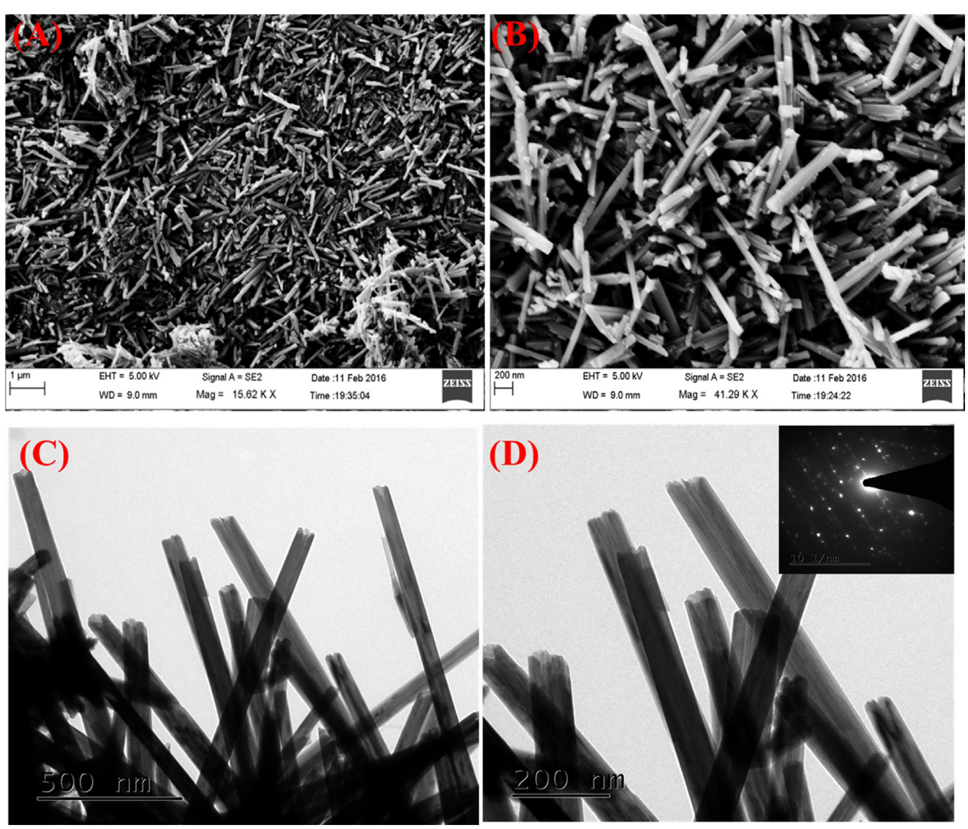

Fig. 2. (A-B) FE-SEM images and (C-D) TEM images of α-MnO_2 nanorods at different magnifications; inset shows the SAED pattern of α-MnO_2 nanorods.

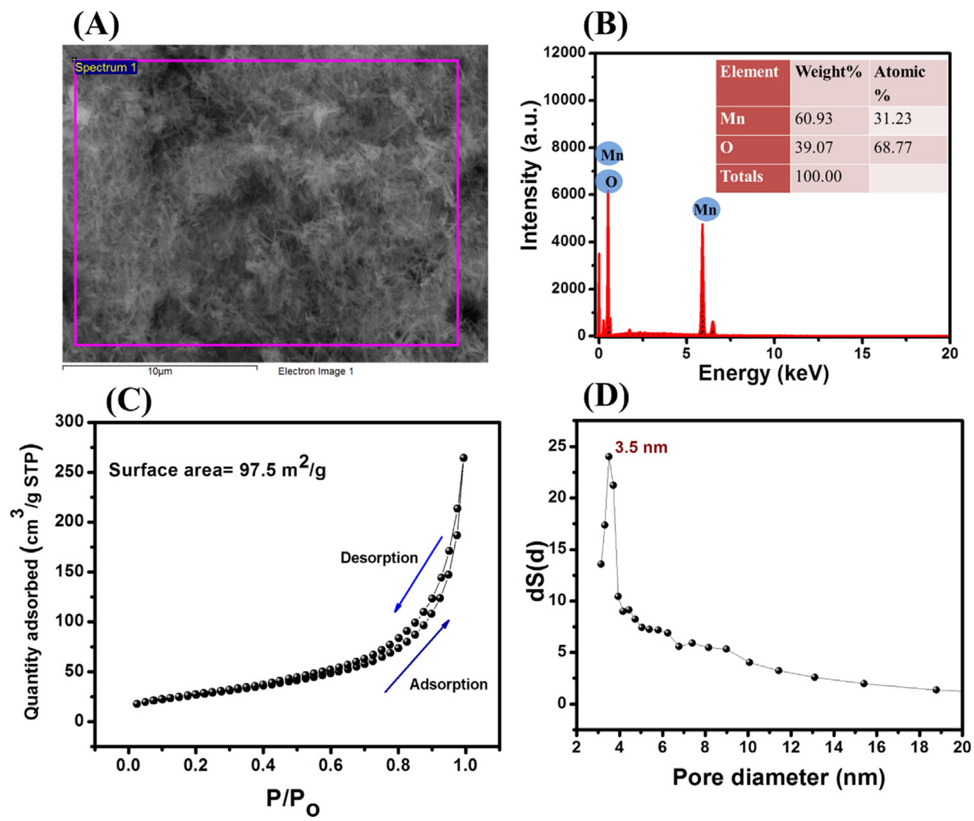

Fig. 3. (A) EDX analysis image, (B) EDX spectrum, (C) N_2 adsorption-desorption isotherm and (D) BJH pore size distribution curve of α-MnO_2 nanorods.

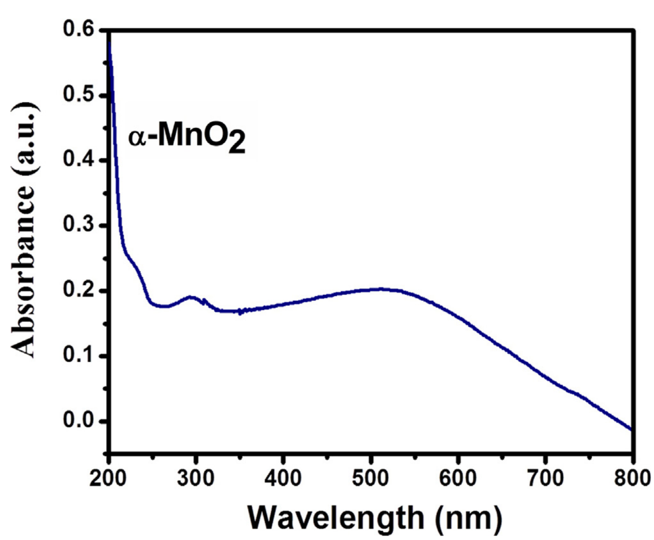

Fig. 4. UV-vis spectrum of α-MnO_2 nanorods.

157.7 (Ω) with a well-defined semi-circle in the medium frequency range. Further, to demonstrate the catalytic activity of the α-MnO_2 nanorods polarization curves and cyclic voltammetry were also employed. Fig. S2(B) showed the polarization curves of the counter electrodes and the slope value at 0 V of α-MnO_2 nanorods was close to that of the Pt. The limiting diffusion current density for the α-MnO_2 nanorods and Pt was found to be 4.01 mA/cm^2 and 4.43 mA/cm^2 which suggest that the catalytic activities of the α-MnO_2 nanorods are comparable to Pt. Furthermore, electrocatalytic ability of the α-MnO_2 nanorods was examined by recording the cyclic voltammetry under I^-/I_3^- electrochemical system using a three electrode system with a scan rate of 50 mV/s. The obtained CV curve clearly showed two typical pairs of redox peaks in which the negative pair was assigned to the oxidation-reduction reaction of I^-/I_3^- (Eq. (1)), while the positive pair correspond to the oxidation-reduction reaction of I_2/I_3^- (Eq. (2)) as shown in Fig. 5.

$$I_3^- + 2e^- \leftrightarrow 3I^- \quad (1)$$

$$3I_2 + 2e^- \leftrightarrow 2I_3^- \quad (2)$$

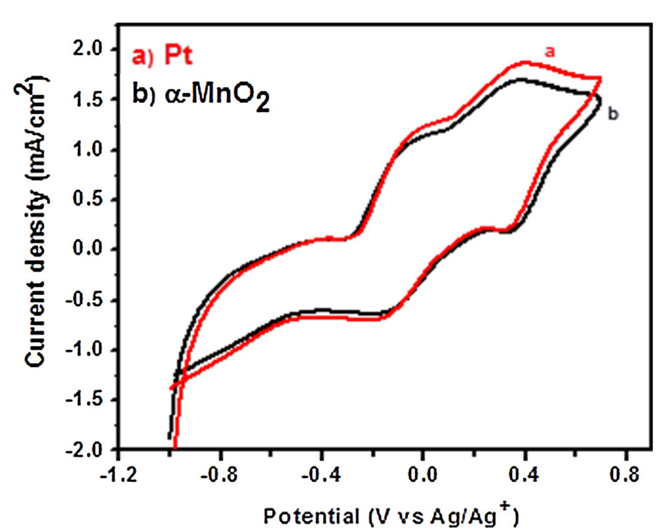

Fig. 5. CV of the triiodide/iodide redox couple for α-MnO_2 based counter electrode (black) and Pt (red).

The role of counter electrode is to catalyze the I_3^- to I^-at the counter electrode/electrolyte interface by collecting the generated electrons from the external circuit.

Additionally, CV curve for Pt counter electrode was also examined to compare the electrocatalytic performance of the α-MnO_2 nanorods as counter electrode. Fig. 5 showed the recorded CV curves of the Pt and α-MnO_2 nanorods based counter electrode which revealed that the α-MnO_2 nanorods shows good electrocatalytic activity as compared to the Pt based electrode. From the obtained results of EIS, polarization curves and CV, it can be concluded that α-MnO_2 nanorods have good electrocatalytic behavior for the reduction of triiodide and may be applied for the fabrication of counter electrode in DSSC. To investigate the stability of the counter electrode fabricated with α-MnO_2 nanorods, cyclic voltammetry was recorded with the 25 consecutive cycles and found no significant changes which suggest excellent stability (Fig. S3(A)) (Scheme 1).

The photocurrent-voltage (*J-V*) characteristics of the fabricated DSSC device were presented in Fig. 6. The DSSC device fabricated with Pt as counter electrodes showed power conversion efficiency (PCE) of 4.7% with (Voc) of 0.71 V, (Jsc) 15.8 mA/cm^2 and (FF) of 0.42, whereas the DSSC device fabricated by employing α-MnO_2 nanorods as counter electrode exhibited a PCE of 4.1% with (Voc) of 0.75 V, (Jsc) 14.7 mA/cm^2 and (FF) of 0.38. These results suggest that α-MnO_2 nanorods can be successfully employed as a counter electrode as an alternative to expensive Pt electrode.

Moreover, the performance of the α-MnO_2 nanorods as a counter electrode in DSSCs was optimized by varying the annealing temperature. Fig. S4 showed the *J-V* characteristics for the devices annealed at 250 °C (Device/250), 300 °C (Device/300), 350 °C (Device/350), 400 °C (Device/400) and 450 °C (Device/450) and the obtained *J-V* parameters are summarized in Table S2. From the observations it was found that the device fabricated with the annealed temperature of 400 °C showed highest performance and this device was consider for further investigation (Fig. 6). In order to study the reproducibility of the optimized DSSC device we have fabricated the three devices and their performances were checked by *I–V* analysis (Fig. S5) and found to be reproducible and the error values for the fabricated DSSCs were presented in Fig. S6. The long term stability of the DSSC device is an important factor in terms of its commercialization. The optimized device was stored for 240 hours and showed no degradation in the performance (Fig. S3(B)). The working of DSSC device can be explained by the following: (i) the incident photon absorbed by the N 719 dye which adsorbed onto the TiO_2 surface, (ii) the excited electron injected to the conduction band of TiO_2 which was further transported to the counter electrode through the circuit and (iii) the transported electron further reached to the redox mediator to regenerate the dye (Scheme 2).

The incident photon-to-electron conversion efficiency (IPCE) of the fabricated devices with Pt and α-MnO_2 nanorods based counter electrode has been examined as shown in Fig. 7. The DSSC fabricated with Pt electrode and the α-MnO_2 nanorods showed a comparable IPCE value which validated the photocurrent obtained for both the devices. Further, the obtained results were compared with reported DSSC and are summarized in Table 1 [6,33–39]. Previously, *Wang* et al. developed the counter electrodes with Ca and NbO_2 which showed good electrocatalytic activity and the PCE for the fabricated DSSC were obtained as 3.43% and 3.62%, respectively. The counter electrodes modified with different materials such as aluminum, SWCNT-PET, Ta_3N_5 NRs and $CoNi_2S_4$ were reported with the PCE in the range of 2.8%-4.61%. Further,

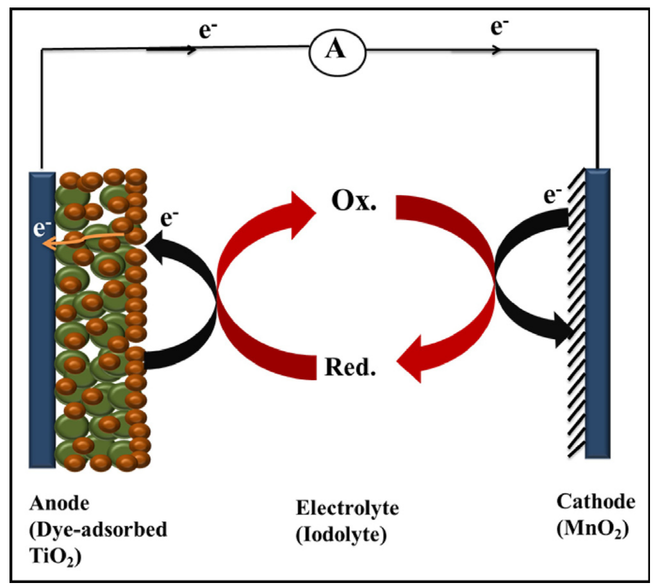

Scheme 2. Schematic representation of the dye sensitized solar cells.

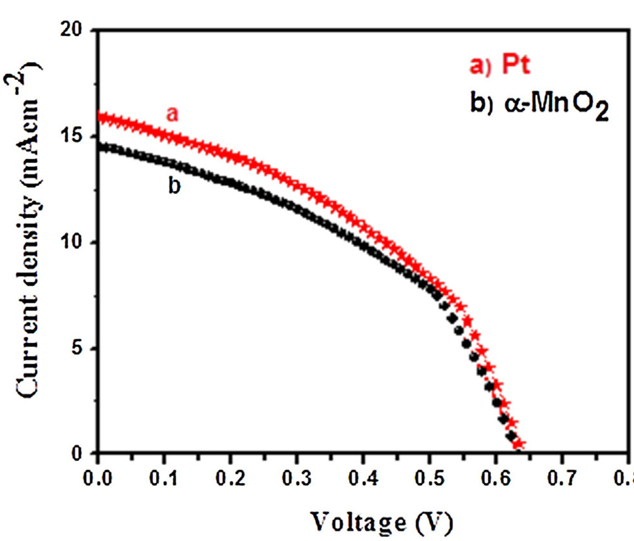

Fig. 6. Photocurrent-voltage (*J-V*) curves of the DSSC with α-MnO_2 based counter electrode (black) and Pt (red).

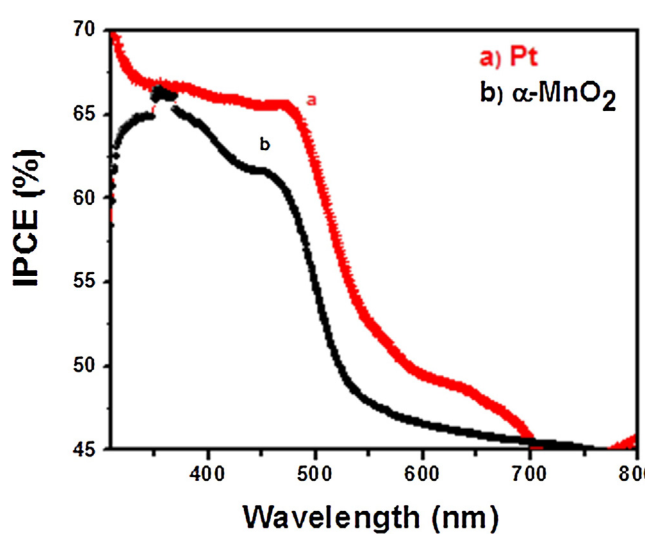

Fig. 7. IPCE curves of the DSSC with α-MnO_2 based counter electrode (black) and Pt (red).

Table 1
Comparison of the performance of α-MnO_2 based DSSC device with previously reported literature.

No.	Counter electrode	J_{sc}(mAcm^{-2})	FF	V_{oc}(V)	η (%)	References
1.	Pt	7.23	0.62	0.65	2.91	[33]
2.	Ca	8.38	0.65	0.63	3.43	[33]
3.	NbO_2	9.14	0.65	0.61	3.62	[33]
4.	Al	10.25	0.42	0.67	2.88	[34]
5.	SWCNT-PET	7.4	0.62	0.80	3.6	[35]
6.	Pt	8.0	0.44	0.50	1.8	[36]
7.	Ta_3N_5 NRs	11.69	0.31	0.78	2.89	[37]
8.	$CoNi_2S_4$	8.86	0.68	0.75	4.61	[38]
9.	rGO	13.47	0.39	0.55	2.93	[6]
10.	rGO/Mn_3O_4	14.73	0.58	0.63	5.4	[6]
11.	α-MnO_2 nanotubes	11.92	0.41	0.67	3.04	[39]
12.	**α-MnO_2nanorods**	**14.7**	**0.38**	**0.65**	**4.1**	***This Work***

Zhang et al. has applied the rGO/Mn_3O_4 based counter electrode which demonstrated the PCE of 5.4%. More recently, *Jin* et al. employed the α-MnO_2 nanotubes which show a low PCE of 3.04%. In this regard, the DSSC device using α-MnO_2 as counter electrode which showed excellent PCE of 4.1% this may be attributed to the mesoporous structure, high porosity/surface area [38] and nanorods like architecture of the synthesized α-MnO_2 nanorods.

3.3. Electrochemical performance of the sensor

Herein, we report involvement of hydrothermally grown α-MnO_2 nanorods towards multipurpose applications such as photovoltaic and sensor. The electrochemical behavior of the α-MnO_2 nanorods modified GCE (**GCE/α-MnO_2**) and bare GCE were investigated in PBS of pH 7.0. Fig. 8(A) depicted the CV of bare GCE and modified **GCE/α-MnO_2** which indicated the current enhancement for **GCE/α-MnO_2** compare to the bare GCE. Subsequently, the bare GCE and **GCE/α-MnO_2** were also investigated on addition of 0.1 μM *p*-nitrotoluene (*p*-NT) which showed enhancement of current with new oxidation and reduction peaks (Fig. 8(B)). From the CVs, it was observed that in addition to irreversible reduction peak (R1) at −0.81 V a pair of new reversible reduction and oxidation peaks at −0.24 V and 0.015 V, respectively were obtained in presence of *p*-NT for the **GCE/α-MnO_2**. The effect of pH on the CVs of *p*-NT was also studied using **GCE/α-MnO_2** in PBS at different pH (Fig. S7). It was observed that with increasing the pH form 2 to 10 the over potential shifted to less positive value and the maximum current was obtained at pH 7.0 therefore, all the studies were performed using PBS of pH 7.0. It is well known that nitroaromatic compounds becomes more explosive with increasing number of nitro groups, thus we have employed **GCE/α-MnO_2** further for the sensing of 2, 4-dinitrotoluene (DNT) and 2, 4, 6-trinitrophenol (TNP) by cyclic voltammetry (Figs. 8C and D). It is to be noted that the highest currents were obtained for modified **GCE/α-MnO_2** electrode as compare to the bare electrode. The effect of varying concentration on the CVs of the nitroaromatic compounds revealed that the current peaks increased linearly with the increase in the concentrations of the nitroaromatic compounds (Fig. 9). The calibration plot of the peak current versus concentration of the nitroaromatic compounds was plotted in inset of Fig. 9.

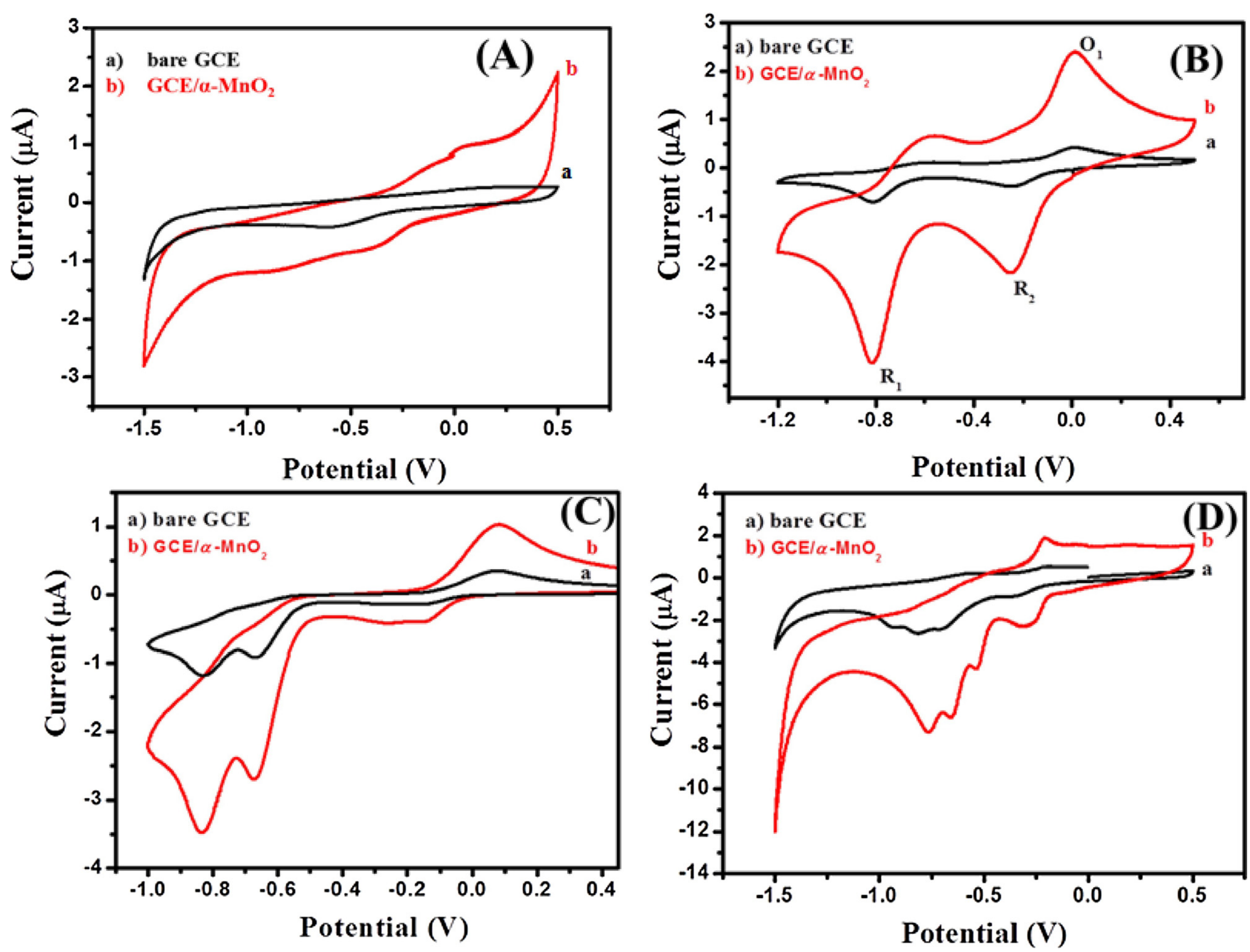

Fig. 8. CV for bare GCE and **GCE/α-MnO_2** in (A) PBS,(B) *p*-NT (C) DNT and (D) TNP at scan rate of 100 mV/s. Conditions: 0.1 M PBS; *p*-NT, DNT and TNP (0.1 μM).

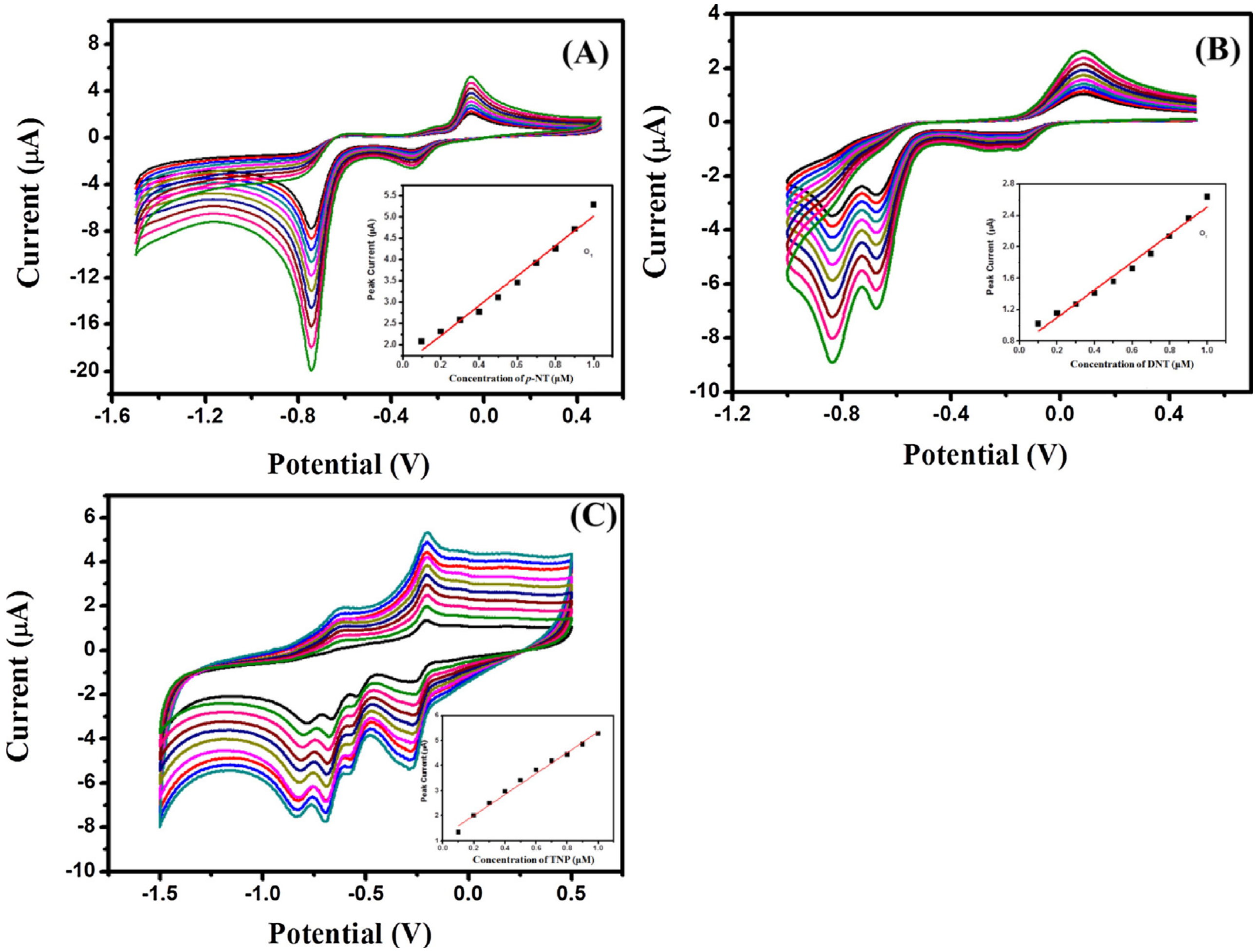

Fig. 9. CV of **GCE/α-MnO₂** for (A) *p*-NT, (B) DNT and (C) TNP at different concentration (0.1–1 μM) in 0.1 M PBS (pH 7.0) at scan rate of 100 mV/s. The calibration plots of peak current against the concentrations are plotted in inset of their respective CV.

Further, the effect of scan rate on the CVs of the nitroaromatic compounds was examined which showed that current peaks increases linearly with increasing the scan rate as confirmed by a linear calibration plot of the scan rate versus current peaks (Fig. S8). Moreover, the differential pulse voltammetry (DPV) was employed for bare GCE and **GCE/α-MnO_2** in the presence of the nitroaromatic compounds which suggest modified **GCE/α-MnO_2** electrode showed a higher current as compared to that of bare GCE and found to be in agreement with the results obtained by cyclic voltammetry (Fig. S9).

To validate these results obtained by CV and DPV, a linear sweep voltammetry (LSV) was introduced to investigate the performance of the **GCE/α-MnO_2** sensor in presence of nitroaromatic compounds (Fig. S10). The result obtained by LSV further confirmed that the **GCE/α-MnO_2** sensor behaved in similar way as demonstrated above by CV and DPV.

3.4. Reproducibility, repeatability and stability of GCE/α-MnO_2 sensor

Four freshly prepared **GCE/α-MnO_2** electrodes were used and their current response towards 0.5 μM of each nitroaromatics in PBS of pH 7.0 with a scan rate of 100 mV/s were recorded and found a negligible variation in current response. Thus, the modified **GCE/α-MnO_2** electrodes could be easily reproducible. The six consecutive cycles of CVs of **GCE/α-MnO_2** were recorded in presence of 0.5 μM *p*-NT using the same electrode and an insignificant variation in current response was observed which revealed that

Table 2
p-NT recovery analysis in real sample.

Sample (Tap Water)	Added amount (μM)	Found	Recovery (%)	RSD(%)
***p*-NT**	0	0	0	0
	0.2	0.18	90.31	3.15
	0.6	0.61	101.43	2.43
	1.0	0.95	95.61	2.91

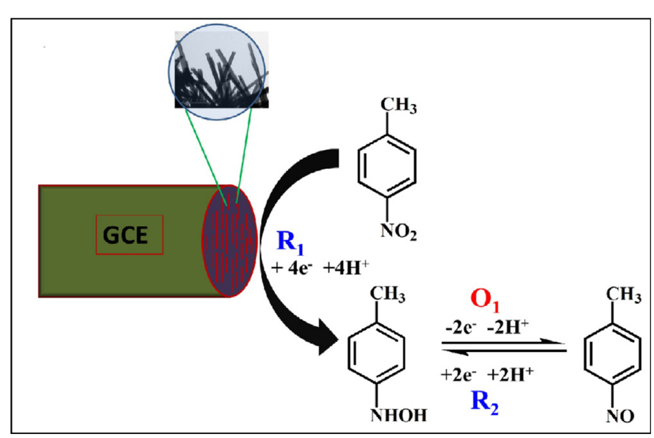

Scheme 3. Proposed mechanism for the sensing of *p*-NT.

Table 3
Comparing of the **GCE/α-MnO$_2$** sensor in terms of LOD, sensitivity and linear range of the nitroaromatic compounds with previously reported sensors.

No.	Electrode	Nitro- aromatic compounds	Limit of detection (LOD) (nM)	Sensitivity	Linear range (μM)	Refs
1.	Screen printed electrode	DNT	700	–	1-200	[40]
2.	Electrochemically Reduced Graphene	DNT	42	–	–	[41]
3.	Sonogel carbon	TNP	2800	–	–	[42]
4.	N-rGO/CuS	TNP	69	–	–	[12]
5.	Functionalized reduced graphene oxide	TNP	540	0.00613 μA/μM	5–215	[13]
6.	**GCE/α-MnO$_2$**	***p*-NT**	**144**	**17.6 μA/μMcm^2**	**0.2–0.8**	***This Work***
		DNT	**133**	**22.6 μA/μMcm^2**	**0.1–0.7**	
		TNP	**100**	**54.82 μA/μMcm^2**	**0.1–1.0**	

the **GCE/α-MnO$_2$** was easily repeatable (Fig. S11). Further, these electrodes when not in use were stored in air at 4 °C and the current response was checked after 30 days and no significant variation were observed in current response which advocated that the present **GCE/α-MnO$_2$** sensor was highly stable.

3.5. Interference study

For any sensor selectivity is very important tool therefore, the selectivity of **GCE/α-MnO$_2$** towards *p*-NT was checked in presence of different interference species (catechol, citric acid, lactose, fructose, Na^+, Mg^{2+}, dopamine, K^+, uric acid, aniline, glucose, resorcinol, phenol and toluene) using chronoamperometry (Fig. S12). A high current response was observed on successive addition of 0.5 and 1 μM *p*-NT whereas an insignificant current response was observed for all other interfering species (20-40% higher). Thus, obtained results indicated that the **GCE/α-MnO$_2$** was highly selective towards the detection of *p*-NT.

3.6. Real sample analysis

The **GCE/α-MnO$_2$** was employed to check the analytical application in real sample water. The tap water was used as real sample and no current response/redox peaks corresponding to the *p*-NT was detected that indicated the absence of *p*-NT in the tap water. Further, 0.2 μM, 0.6 μM and 1 μM were added to the tap water and the cyclic voltammetry was performed which showed the acceptable recovery in the range of 90.3-101.43% of the added *p*-NT (Table 2).

3.7. Mechanism of the GCE/α-MnO$_2$ sensor

Scheme 3 showed the proposed mechanism (where, O_1 and R_1, R_2 represents oxidation and reductions, respectively). The first redox reaction occurred due to reduction of *p*-NT to *p*-hydroxylamino-toluene (R_1) followed by the oxidation of *p*-hydroxylamino-toluene to the *p*-nitroso-toluene (O_1) with the subsequent reversible reduction (R_2) (Fig. 8(B)).

The sensitivity and performances of the **GCE/α-MnO$_2$** sensor for different nitroaromatic compounds were obtained by calculating the limit of detection (LOD) and sensitivity by using equations, LOD = 3.3(σ/S) [Where σ is standard error and S is the slope of calibration curve] and Sensitivity = Slope/Area of the electrode and the results obtained are summarized in Table 3 [12,13,40–42]. It is to be noted that the **GCE/α-MnO$_2$** showed better LOD, linearity and sensitivity for TNP among other nitroaromatic compounds.

There exist several reports on the detection of nitroaromatic compounds by employing various methods such as photoluminescence, coulometry and chromatography etc [16], but only few reports available on electrochemical sensors [13]. Previously, *Caygill* et al. proposed the electrochemical sensor for the detection of DNT using simple screen printed electrode with a detection limit of 700 nM. Further, *Chen* et al. *and del Mar* et al. fabricated the electrochemical sensor for the detection of DNT by employing carbon materials (rGO and sonogel carbon) which showed the detection limits of 42 nM and 2800 nM, respectively. In other reports, the functionalized rGO and nitrogen doped rGO/copper sulfide composite were proposed to fabricate the electrodes for electrochemical detection of TNP. These electrodes showed the limit of detection of 540 nM and 69 nM respectively. Although these reported sensor showed good performance but still a highly sensitive and selective sensor with excellent detection limit remained a challenge for practical applications. Furthermore, most of the sensors have been proposed to sense the individually nitroaromatic compound. Thus, our **GCE/α-MnO$_2$** sensor has an edge over in terms of the following observation (i) binder free, (ii) low cost, (iii) low limit of detection and (iv) high sensitivity as compared to most of the reported sensor (Table 3). Moreover, to the best of our knowledge so far no report was found on the detection of three selected nitroaromactic compounds (*p*-NT, DNT and TNP) by employing single modified electrode (**GCE/α-MnO$_2$**) with various techniques such as CV, DPV and LSV.

From Table 3 it was observed that the proposed **GCE/α-MnO$_2$** sensor had high sensitivity which may be due the high surface area of the synthesized α-MnO_2 nanorods. Additionally, this **GCE/α-MnO$_2$** sensor showed good reproducibility, repeatability, selectivity and stability which make it superior over reported sensors.

4. Conclusion

To summarize, we report facile synthetic route for preparation of α-MnO_2 nanorods which showed multi-talented features. These α-MnO_2 nanorods were employed as a low cost counter electrode for (i) DSSC which showed remarkable PCE of 4.1% and (ii) for sensing of a series of nitro aromatics in particular TNP which is well known as an explosive. The binder free **GCE/α-MnO$_2$** sensor showed good electro-catalytic response, low detection limit and high sensitivity towards the detection of nitroaromatic compounds. The α-MnO_2 nanorods based DSSCs and modified electrode performances were compared with those of other reported materials and found to be superior.

Acknowledgements

K. A. would like to thanks to University Grant Commission (UGC) New Delhi, India for providing fellowship (RGNF-D). S.M.M. thanks SERB-DST (Project No. EMR/2016/001113), New Delhi, India for financial support. We sincerely acknowledge Sophisticated Instrumentation Centre (SIC), IIT Indore for providing the characterization facility. We thank the Advanced Imaging Center, IIT Kanpur for providing TEM facility.

Appendix A. Supplementary data

Supplementary data associated with this article can be found, in the online version, at http://dx.doi.org/10.1016/j.electacta.2017.09.010.

References

[1] K.G. Reddy, T.G. Deepak, G.S. Anjusree, Sara Thomas, Sajini Vadukumpully, K.R. V. Subramanian, Shantikumar, V. Nair, A. Sreekumaran Nair, On global energy scenario, dye-sensitized solar cells and the promise of nanotechnology, Phys. Chem. Chem. Phys 16 (2014) 6838–6858.

[2] V. Sundararajana, G. Selvaraj, H.M. Ng, S. Ramesh, K. Ramesh, C.D. Wilfred, S. Bashir, Exploring the effect of novel N-butyl-6-methylquinolinium bis (trifluoromethylsulfonyl)imide ionic liquid addition to poly(methyl methacrylate-co-methacrylic) acid electrolyte system as employed in gel-state dye sensitized solar cells, Electrochim. Acta 240 (2017) 361–370.

[3] P. Sun, T. Huang, Z. Chen, L. Tian, H. Huang, N. Huang, S. Zhou, M. Long, Y. Sun, X. Sun, Solution Processed NixSy Films: Composition Morphology and Crystallinity Tuning via Ni/S-Ratio-Control and Application in Dye-Sensitized Solar Cells, Electrochim. Acta 246 (2017) 285–293.

[4] Y. Liu, S. Yun, X. Zhou, Y. Hou, T. Zhang, J. Li, A. Hagfeldt, Intrinsic Origin of Superior Catalytic Properties of Tungsten-based Catalysts in Dye-sensitized Solar Cells, Electrochim. Acta 242 (2017) 390–399.

[5] J. Theerthagiri, R.A. Senthil, M.H. Buraidah, J. Madhavan, A.K. Arof, M.A. kumar, One-step electrochemical deposition of $Ni_{1-x}Mo_xS$ ternary sulfides as an efficient counter electrode for dye-sensitized solar cells, J. Mater. Chem. A 4 (2016) 16119–16127.

[6] Q. Zhang, Y. Liu, Y. Duan, N. Fu, Q. Liu, Y. Fang, Q. Sun, Y. Lin, Mn_3O_4/graphene composite as counter electrode in dye-sensitized solar cells, RSC Adv. 4 (2014) 15091–15097.

[7] J. Yang, C. Bao, K. Zhu, T. Yu, F. Li, J. Liu, Z. Li, Z. Zou, High catalytic activity and stability of nickel sulfide and cobalt sulfide hierarchical nanospheres on the counter electrodes for dye-sensitized solar cells, Chem. Commun. 50 (2014) 4824–4826.

[8] C. Bora, C. Sarkar, K.J. Mohan, S. Dolui, Polythiophene/graphene composite as a highly efficient platinum-free counter electrode in dye-sensitized solar cells, Electrochim. Acta 157 (2015) 225–231.

[9] T. Sinha, M. Ahmaruzzaman, A. New, Facile Strategy for the One-pot Fabrication of Luminescent Gold Nanoclusters and their Prospective Application, RSC Adv. 6 (2016) 44–56.

[10] S. Pandey, S.B. Mishra, Catalytic Reduction of *p*-nitrophenol by Using Platinum Nanoparticles Stabilised by Guar Gum, Carbohydr. Polym. 113 (2014) 525–531.

[11] R. Arasteh, M. Masoumi, A. Rashidi, L. Moradi, V. Samimi, S. Mostafavi, Adsorption of 2-Nitrophenol by Multi-wall Carbon Nanotubes from Aqueous Solutions, Appl. Surf. Sci. 256 (2010) 4447–4455.

[12] K. Giribabu, S.Y. Oh, R. Suresh, S.P. Kumar, R. Manigandan, S. Munusamy, G. Gnanamoorthy, J.Y. Kim, Y.S. Huh, V. Narayanan, Sensing of Picric Acid with a Glassy Carbon Electrode Modified with CuS Nanoparticles Deposited on Nitrogen-Doped Reduced Graphene Oxide, Microchim. Acta 183 (2016) 2421–2430.

[13] J. Huang, L. Wang, C. Shi, Y. Dai, C. Gu, J. Liu, Selective Detection of Picric Acid Using Functionalized Reduced Graphene Oxide Sensor Device, Sens. Actuators B Chem. 196 (2014) 567–573.

[14] W. Zhang, C.R. Wilson, N.D. Danielson, Indirect fluorescent determination of selected nitro-aromatic and pharmaceutical compounds via UV-photolysis of 2-phenylbenzimidazole-5-sulfonate, Talanta 74 (2008) 1400–1407.

[15] J.A. Padilla-Sa'nchez, P. Plaza-Bolaños, R. Romero-Gonza'lez, A. GarridoFrenich, J.L.M. Vidal, Application of a quick easy, cheap, effective, rugged and safe-based method for the simultaneous extraction of chlorophenols, alkylphenols, nitrophenols and cresols in agricultural soils, analyzed by using gas chromatography-triple quadrupole-mass spectrometry/mass spectrometry, J. Chromatogr. A 1217 (2010) 5724–5731.

[16] S.P. Wang, H.J. Chen, Separation and determination of nitrobenzenes by micellar electrokinetic chromatography and high-performance liquid chromatography, J. Chromatogr. A 979 (2002) 439–446.

[17] X. Guo, Z. Wang, S. Zhou, The separation and determination of nitrophenol isomers by high-performance capillary zone electrophoresis, Talanta 64 (2004) 135–139.

[18] Y. Tang, R. Huang, C. Liu, S. Yang, Z. Lu, S. Luo, Electrochemical detection of 4-nitrophenol based on a glassy carbon electrode modified with a reduced graphene oxide/Au nanoparticle composite, Anal. Methods 5 (2013) 5508–5514.

[19] A.M. O'Mahony, J. Wang, Nanomaterial-based electrochemical detection of explosives: a review of recent developments, Anal. Methods 5 (2013) 4296–4309.

[20] Y. Tang, R. Huang, C. Liu, S. Yang, Z. Lu, S. Luo, Electrochemical detection of 4-nitrophenol based on a glassy carbon electrode modified with a reduced graphene oxide/Au nanoparticle composite, Anal. Methods 5 (2013) 5508–5514.

[21] P. Zhang, M. He, S. Xu, X. Yan, The controlled growth of porous d-MnO_2 nanosheets on carbon fibers as a bi-functional catalyst for rechargeable lithium?oxygen batteries, J. Mater. Chem. A 3 (2015) 10811–10818.

[22] D. Wang, L. Liu, S. Zhao, B. Li, H. Liu, X.F. Lang, β-MnO_2 as a Cathode Material for Lithium Ion Batteries from First Principles Calculations, Phys. Chem. Chem. Phys 15 (2013) 9075–9083.

[23] Y. Dai, L. Chen, V. Babayan, Q. Cheng, P. Saha, H. Jiang, C. Li, Ultrathin MnO_2 Nanoflakes Grown on N-doped Carbon Nanoboxes for High-energy Symmetric Supercapacitors, J. Mater. Chem. A 3 (2015) 21337–21342.

[24] T. Zhai, X. Lu, F. Wang, H. Xia, Y. Tong, MnO_2 Nanomaterials for Flexible Supercapacitors: Performance Enhancement *via* Intrinsic and Extrinsic Modification, Nanoscale Horiz. 1 (2016) 109–124.

[25] X. Guo, J. Han, L. Zhang, P. Liu, A. Hirata, L. Chen, T. Fujita, M. Chen, A nanoporous metal recuperated MnO_2 anode for lithium ion batteries, Nanoscale 7 (2015) 15111–15116.

[26] M. Huang, F. Li, F. Dong, Y.X. Zhang, L.L. Zhang, MnO_2-based Nanostructures for High-performance Supercapacitors, J. Mater. Chem. A 3 (2015) 21380–21423.

[27] B. Yin, S. Zhang, Y. Jiao, Y. Liu, F. Qu, X. Wu, Facile Synthesis of ultralong MnO_2 Nanowires as High Performance Supercapacitor Electrodes and Photocatalysts with Enhanced Photocatalytic Activities, Cryst Eng Comm. 16 (2014) 9999–10005.

[28] D. Su, H.-J. Ahn, G. Wang, Hydrothermal synthesis of α-MnO_2 and β-MnO_2 nanorods as high capacity cathode materials for sodium ion batteries, J. Mater. Chem. A 1 (2013) 4845–4850.

[29] W. Yu, X. Jiang, S. Ding, B.Q. Li, Preparation and electrochemical characteristics of porous hollow spheres of NiO nanosheets as electrodes of supercapacitors, J. Power Sources 256 (2014) 440–448.

[30] J. Dong, J. Wu, J. Jia, S. Wu, P. Zhou, Y. Tu, Z. Lan, Cobalt selenide nanorods used as a high efficient counter electrode for dye-sensitized solar cells, Electrochim. Acta 168 (2015) 69–75.

[31] S. Yang, X. Song, P. Zhang, L. Gao, Facile Synthesis of Nitrogen-Doped Graphene-Ultrathin MnO2 Sheet Composites and Their Electrochemical Performances, ACS Appl. Mater. Interfaces 5 (2013) 3317–3322.

[32] P. Vijayakumar, M. Senthil Pandian, S.P. Lim, A. Pandikumar, N.M. Huang, S. Mukhopadhyay, P. Ramasamy, Facile synthesis of tungsten carbide nanorods and its application as counter electrode in dye sensitized solar cells, Mat. Sci. in Semicon. Proc 39 (2015) 292–299.

[33] L. Wang, E.W.-G. Diau, M. Wu, H.-P. Lu, T. Ma, Highly efficient catalysts for Co(II/III) redox couples in dye-sensitized solar cells, Chem. Commun. 48 (2012) 2600–2602.

[34] P. Chal, A. Shit, A.K. Nandi, Dye-sensitized Solar Cell from a New Organic n-type Semiconductor/Polyaniline Composite: Insight from Impedance Spectroscopy, J. Mater. Chem. C 4 (2016) 272–285.

[35] K. Aitola, J. Halme, S. Feldt, P. Lohse, M. Borghei, A. Kaskela, A.G. Nasibulin, E.I. Kauppinen, P.D. Lund, G. Boschloo, A. Hagfeldt, Highly catalytic carbon nanotube counter electrode on plastic for dye solar cells utilizing cobalt-based redox mediator, Electrochim. Acta 111 (2013) 206–209.

[36] F. Ghamouss, R. Pitson, F. Odobel, M. Boujtita, S. Caramoric, C.A. Bignozzic, Characterization of screen printed carbon counter electrodes for Co(II)/(III) mediated photoelectrochemical cells, Electrochim. Acta 55 (2010) 6517–6522.

[37] Yan Li, Q. Feng, H. Wang, G. Zhou, Z.-S. Wang, Reduced graphene oxide–Ta_3N_5 composite: a potential cathode for efficient $Co(bpy)_3^{3+/2+}$ mediated dye-sensitized solar cells, J. Mater. Chem. A 1 (2013) 6342–6349.

[38] Z. Shi, K. Deng, L. Li, Pt-free and efficient counter electrode with nanostructured $CoNi_2S_4$ for dye-sensitized solar cells, Sci Rep. 5 (2015) 9317.

[39] P. Jin, X. Zhang, M. Zhen, J. Wang, MnO_2 nanotubes with graphene-assistance as lowcost counter-electrode materials in dye-sensitized solar cells, RSC Adv 6 (2016) 10938–10942.

[40] J.S. Caygill, S.D. Collyer, J.L. Holmes, F. Davisa, S.P.J. Higson, Disposable Screen-printed Sensors for the Electrochemical Detection of TNT and DNT, Analyst 138 (2013) 346–352.

[41] T.W. Chen, Z.H. Sheng, K. Wang, F.B. Wang, X.H. Xia, Determination of Explosives Using Electrochemically Reduced Graphene, Chem. Asian J 6 (2011) 1210–1216.

[42] R.M. del Mar, I.N. Rodríguez, J.M. Palacios-Santander, L.M. Cubillana-Aguilera, J. L. Hidalgo-Hidalgo-de-Cisneros, Study of the Responses of a Sonogel-Carbon Electrode Towards Phenolic Compounds, Electroanal 17 (2005) 806–814.